Int J Adv Manuf Technol (2017) 88:2773–2783
DOI 10.1007/s00170-016-8993-6

ORIGINAL ARTICLE

Dissimilar welding of A7075-T651 and AZ31B alloys by gas metal arc plug welding method

M. R. Islam[1] · **M. Ishak**[1] · **L. H. Shah**[1] · **S. R. A. Idris**[1] · **C. Meriç**[2]

Received: 2 December 2015 / Accepted: 30 May 2016 / Published online: 8 June 2016

Abstract Innovative welding techniques allow for the fabrication of light, high-specific-strength, and fuel-saving Al and Mg alloys for use in transportation industries. Furthermore, these techniques have minimal detrimental impact on the environment. However, the poor mechanical properties of joints resulting from the formation of brittle Al_mMg_n intermetallic compounds are key barriers to joining Al and Mg alloys. To date, a proper solution to this problem has not yet been provided. The aim of this research was to investigate the mechanical and metallurgical properties of the joint between AZ31B and A7075-T651 alloys welded by a new technique called gas metal arc plug welding method. ER5356 aluminum wire was used as a filler. The yield and ultimate tensile strengths as well as impact toughness of the joints were measured. The fracture surface was investigated by scanning electron microscopy and energy-dispersive X-ray spectroscopy. The maximum ultimate tensile strength and impact toughness of the joints were 89 and 84 % of those of the AZ31B parent alloy, respectively. Generally, the joints failed in the ER5356 nugget, whereas some failed in the AZ31B alloy. No fracture was observed in the A7075-T65 alloy. Brittle fracture mechanism was observed for all the joints. In conclusion, the proposed welding technique can allow for better mechanical properties of joints for dissimilar welding of aluminum and magnesium alloys.

Keywords A7075-T651 · AZ31B · Strength · Fracture toughness · Gas metal arc · Plug

1 Introduction

Lightweight structures are of primary importance in the automotive, aviation, aerospace, and marine industries because they can reduce fuel consumption and greenhouse gas emissions [1]. Although steel is the principal material used in transportation industries, such materials as Al and Mg have drawn considerable attention because of their lightweight and fuel-saving properties [2]. Accordingly, researchers have searched for high-strength and fuel-efficient (i.e., lightweight) metals [3]. At present, Al and Mg are classified as the lightest and most important nonferrous metals, as well as the most promising materials in manufacturing industries [4]. Alloys from both metals have been continuously and extensively researched during the past decades because of their practical industrial applications. In fact, various Al and Mg alloys are anticipated to become the fundamental materials in almost all structures in the near future. In most land, water, and air transportation systems, particularly in the automotive industry, both Al and Mg alloys are used in the structures of the aforementioned systems. Thus, a successful welding technique is of utmost importance to combine these two alloys [5]. The main difficulties in welding these two alloys result from the differences in their physical and chemical properties. Moreover, Al–Mg reaction causes the formation of very brittle and fragile Al_mMg_n-type intermetallic compounds (IMCs). Consequently, the joint formed with these two alloys possesses very low strength, and it can be easily fractured, even

✉ M. Ishak
mahadzir@ump.edu.my

[1] Faculty of Mechanical Engineering, Universiti Malaysia Pahang, Pekan 26600, Pahang, Malaysia

[2] Mechanical Engineering Department, Fatih University, Istanbul, Turkey

by hand. An appropriate welding technique that can reduce or avoid the formation of Al_mMg_n IMCs in the welding joint should be introduced to achieve a joint with good mechanical and metallurgical properties [5].

Both Al and Mg alloys possess numerous attractive physical, mechanical, and chemical properties, such as light weight, excellent thermal conductivity and electrical conductivity, high specific strength, high stiffness, good formability, high durability, recyclability, excellent corrosion resistance, low-cost maintenance, and high recovery potential [3, 4]. With the requirements for fuel economy and environmental conservation, specific strength is and will continue to be a key factor in material selection [5]. Recently, numerous industries have shown considerable interest to Al and Mg alloys for their potential usability in an extensive array of applications. To enhance the properties of these alloys and develop innovative and reliable welding technologies, several scholars [6] have investigated the use of these two alloys in compound structures to reduce vehicle weight and cost and achieve better mechanical properties, particularly in key engineering applications, such as automotive [7], marine [8], aviation, aerospace [9], and electronics [2, 8, 10, 11]. Given the extensive use of these alloys as structural materials, innovative ways to join them are essential [5, 12–16]. Joining these two alloys may allow for enhanced design flexibility and quality of components through compound structures [17]. Furthermore, joining by welding of Mg and Al alloys can improve the flexibility and availability of several components substantially [7]. Accordingly, the effectiveness of the joint between Al and Mg alloys should be investigated. In addition, problems in Al and Mg welding must be addressed and solved [12, 16].

The application of modern industrial materials has also made the welding technology for Al and Mg alloys important [17]. Welding joints significantly affect the life span, safety, endurance, and quality of structures [2]. They are also highly considered in a wide range of applications of advanced materials, such as Al and Mg alloys. At present, gas metal arc (GMA), friction stir welding (FSW), tungsten inert gas (TIG), laser, hybrid laser/TIG, neodymium-doped yttrium–aluminum garnet, explosive, resistance spot welding (RSW), cold metal transfer, and electron beam welding methods have been utilized for joining both alloys [10, 18–20]. Few unconventional approaches, including vacuum diffusion bonding and hybrid FSW, have been tried to enhance the mechanical properties of welding joints. However, most of the attempts achieved either partially satisfactory or unsatisfactory results because Al_2Mg_3-, Mg_2Al_3-, and $Mg_{17}Al_{12}$-type IMCs are formed at the Al–Mg interface. These IMCs are incredibly brittle and degrade the mechanical properties of the joints [15, 21, 22]. Certain welding configurations and the selection of appropriate parameters within appropriate ranges could be among the solutions to reduce or inhibit the formation of Al_mMg_n IMCs. The maximum strength of the welding joint between Al and Mg alloys achieved thus far is only 67 % of the maximum strength of the Al-based alloy, which is very low [16]. Therefore, extensive research should be undertaken to establish reliable welding techniques between Al and Mg alloys.

To address the aforementioned problems and enhance the traditional GMA welding technique [10, 23, 24], the current study presented a new GMA plug welding method using ER5356 Al filler to join A7075-T651 and AZ31B alloys. GMA plug welding is similar to welding in single-point through holes without moving the workpiece or welding gun. In this joining method, the lower and upper pieces are in a lap configuration. A lap joint is one of the most common joint shapes in the automotive and aviation industries, and it is normally achieved using the RSW method. However, using RSW to weld any Al alloy to any Mg alloy causes the formation of Al_mMg_n-type IMCs, which deteriorate the essential mechanical properties of the joint [25]. By contrast, the proposed technique can minimize the formation of Al_mMg_n IMCs by reducing the direct bonding area between the Al and Mg alloys to improve the mechanical properties of the joint, such as yield strength (YS), ultimate tensile strength (UTS), and fracture toughness. GMA plug welding method can also expedite the combination and extensive use of Al and Mg alloys in the mass production of lightweight vehicle structures in the marine, automotive, aviation, and aerospace industries. Therefore, in this study, the UTS and impact toughness of the joint between A7075-T651 Al and AZ31B Mg alloys were examined. Metallurgical investigations of the fracture surface and welding cross sections were also conducted by optical microscopy, scanning electron microscopy (SEM), and energy-dispersive X-ray spectroscopy (EDX).

2 Research methodology

2.1 Experimental method

From A7075-T651 and AZ31B alloy sheets, 75 × 70 × 2 mm (length × width × depth) plates were cut by a shear-cutting machine. Then, 3.5-mm-diameter holes were drilled in each Al and Mg plate, as shown in Fig. 1. The alloy plates were rubbed on flat mechanical files to refine and polish the edges. Each plate was then polished using 360-grit emery paper to remove the oxide films on the faying surfaces. Before welding, the pieces were wiped with an acetone solution to remove impurities, such as oil and grease, which are typically present after cutting and drilling processes. The AZ31B alloy plate was placed on top of the A7075-T651 alloy plate, overlapping by 20 mm. The shielding gasses used were 98 % Ar + 2 % O_2 throughout the welding process. First, the GMA plug welding was applied to the through holes on the A7075-T651 side. Subsequently, the A7075-T651 side was positioned facing

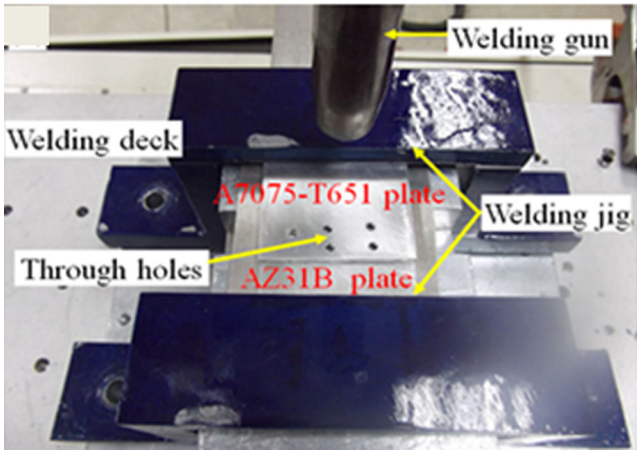

Fig. 1 Illustration of the welding layout

downward to weld the AZ31B alloy side. The welding time was 5 s for the A7075-T651 alloy side and 3 s for the AZ31B alloy side. The chemical compositions of the parent alloys and the filler material are shown in Table 1.

The design of experiments (DOE) was completed by the Box–Behnken technique of the response surface method. The DOE and the welding powers are shown in Table 2. Twenty-six sets of experimentations were completed in replicate based on the DOE.

From the welded workpieces, tensile and toughness specimens were prepared by EDM wire cutting machine according to standard dimensions. Tensile test specimens complied with the ASTM E8M-04 standard (length 100 mm; grip length 20 mm; grip width 20 mm; gauge length 40 mm; width of reduced section 12.5 mm; fillet radius of reduced section 12.5 mm) [26]. The specimens were tested in an INSTRON universal testing machine at room temperature and a strain rate of 2 mm/min with 50 kN load to determine the YS and UTS of the welding joints. Impact toughness specimens were prepared according to the ASTM D5045 standard (length 55 mm; width 10 mm; U-notch depth 2 mm; U-notch width 0.5 mm; notch root radius 0.25 mm) and tested in a Zwick Roell digital impact tester to determine the absorbed impact energy (CVN) of the joint [27]. The test was performed with a 15-J capacity and 390-mm-long pendulum. The angle of release was 160°, and room temperature means 30 °C [28].

Table 1 Chemical compositions of A7075-T651, AZ31B alloys and ER5356 Al fillers (wt %) [24–30]

Element	A7075-T651	AZ31B	ER5356
Al	Balance	2.5–3.5	Balance
C	–	–	–
Ca	–	0.04	–
Co	–	–	–
Cr	0.23	–	0.06
Cu	1.6–1.8	–	0.011
Fe	0.50	–	0.20
Mg	2.5–2.7	Balance	4.6–5.0
Mn	0.30	<1.0	0.15
Mo	–	–	–
Ni	–	–	–
Si	0.40	<0.20	0.20
Ti	0.20	–	>0.05
Zn	5.6	0.5–2.0	>0.10

Welding an Al alloy to a Mg alloy is an entirely new method and has not been documented. In this new method, an ER5356 Al filler was used because of its moderate strength and toughness and compatibility with both A7075-T651 and AZ31B alloys. The ER5356 Al filler were formed into nuggets in the through holes to affix the two alloys strongly. Thus, the two dissimilar alloys were joined through the ER5356 Al nuggets and the direct bonding area. Through this method, the formation of Al_mMg_n-type IMCs was minimized during the welding of these two alloys. Consequently, failure would most probably occur on the weakest AZ31B alloy side or the relatively weak ER5356 Al nugget side. In this study, the maximum attainable joint fracture toughness was targeted.

3 Results and discussion

3.1 Comparison of the strength and impact toughness of the joint

YS, UTS, and absorbed impact energy (CVN) values are tabulated in Table 2. As shown in Table 2, the joint fabricated at a gas-flow rate (GSR) of 15 L/min, tip-to-work distance (TWD) of 10 mm, welding voltage (WV) of 20 V, and welding current (WC) of 115 A achieved the lowest YS (57.28 MPa). By contrast, the joint fabricated at a GSR of 5 L/min, TWD of 10 mm, WV of 15 V, and WC of 115 A achieved the highest YS (176.30 MPa). The joint fabricated at a GSR of 15 L/min, TWD of 10 mm, WV of 10 V, and WC of 65 A achieved the lowest UTS (61.19 MPa). By contrast, the joint fabricated at a GSR of 15 L/min, TWD of 8 mm, WV of 15 V, and WC of 115 A achieved the highest UTS (226.28 MPa, which is 89.07 % of the UTS of the AZ31B parent alloy). The joint fabricated at a GSR of 5 L/min, TWD of 10 mm, WV of 20 V, and WC of 90 A achieved the lowest impact toughness as indicated by CVN (1.8 J). On the contrary, the joint fabricated at a GSR of 15 L/min, TWD of 8 mm, WV of 15 V, and WC of 115 A achieved the highest impact toughness (7.42 J, which is 85.5 % of the impact toughness of the AZ31B parent alloy). Thus, the recommended welding parameters for the novel welding method are 15 L/min GSR, 8 mm TWD, 15 V WV, and 115 A WC as they allow for high tensile strength and good impact toughness. Consequently, better and significantly improved mechanical properties were achieved with the use of

Table 2 Design of experiments and welding power

Exp. No.	GSR/ (Lmin^{-1})	TWD (mm)	WV (V)	WC (A)	Welding Power (V × C), Watt	Yield strength, YS (MPa)	Ultimate tensile strength (MPa)	Impact energy, CVN (J)
1	5	8	15	90	1350	144.05	204.14	5.33
2	25	8	15	90	1350	98.080	112.65	3.92
3	5	12	15	90	1350	107.02	112.15	3.93
4	25	12	15	90	1350	135.54	177.78	5.41
5	15	10	10	65	650	59.640	61.190	3.18
6	15	10	20	65	1300	80.840	101.68	2.54
7	15	10	10	115	1150	119.03	155.00	4.29
8	15	10	20	115	2300	57.280	70.770	1.95
9	5	10	15	65	975	89.490	104.69	3.65
10	25	10	15	65	975	126.86	147.82	4.93
11	5	10	15	115	1725	176.30	193.00	4.92
12	25	10	15	115	1725	88.035	117.38	4.27
13	15	8	10	90	900	81.060	111.89	3.26
14	15	12	10	90	900	104.99	128.74	4.81
15	15	8	20	90	1800	79.370	122.10	3.15
16	15	12	20	90	1800	72.190	73.630	1.86
17	15	10	15	90	1350	108.79	109.57	3.89
18	5	10	10	90	900	98.350	106.57	3.68
19	25	10	10	90	900	65.680	84.780	3.16
20	5	10	20	90	1800	48.180	81.170	1.83
21	25	10	20	90	1800	83.340	70.770	2.22
22	15	8	15	65	975	98.960	121.36	4.08
23	15	12	15	65	975	121.26	178.24	5.66
24	15	8	15	115	1725	97.870	226.28	7.42
25	15	12	15	115	1725	111.17	136.11	4.77
26	15	10	15	90	1350	75.820	112.35	4.97
A7075	–	–	–	–	–	464.87	590.05	8.82
AZ31B	–	–	–	–	–	203.63	254.05	8.67

an Al filler. Most of the welding joints failed in the Al nugget. The strengths of AZ31B (σ_s, 220–290 MPa) or A7075-T651 (σ_s, 570 MPa) parent alloys were each higher than that of the ER5356 Al filler (σ_s, 265 MPa), and the strength of the Al filler was considered the strength of the joints. The joints achieved better mechanical properties mainly because these joints were fabricated at a medium welding power (1725 W), which resulted in the proper melting, bonding, and formation of fine grains and precipitates. Less pores, voids, and cracks also formed at a medium welding power. By contrast, a low welding power resulted in a lack of fusion and improper bonding, whereas a high welding power caused coarse grains in the fusion zone and the formation of voids, pores, cracks, oxides, and burn-throughs [29].

Figure 2 illustrates the mechanical properties of the welding joints through the stress–strain curves generated by tensile testing and compares the curves with those of the parent alloys. In this study, only the stress–strain curves for the minimum and maximum UTSs were considered. From the stress–strain curves, the YS and UTS of any joint can be

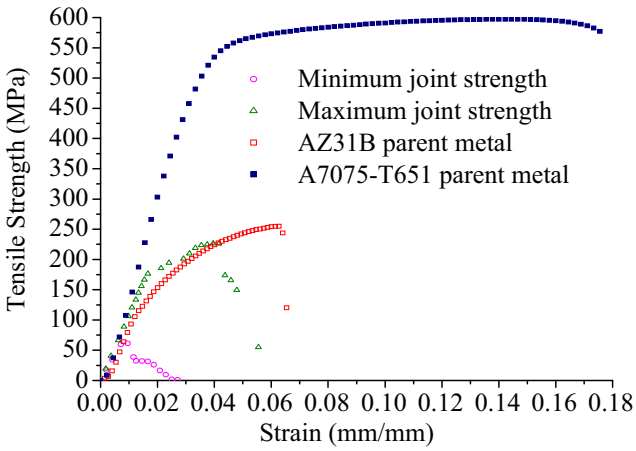

Fig. 2 Comparison of stress strain curves for joints with minimum and maximum UTS and parent metals

derived. As shown in Fig. 2, the curves of the joints with minimum and maximum UTSs both exhibited lower elongation and lower stress level than those of their AZ31B and A7075-T651 parent alloys before reaching UTS. This result proved that both joints exhibited lower plasticity but the joint with the maximum UTS had higher elongation and higher plasticity than the joint with the minimum UTS. This result also proved that the Al filler had lower ductility [30].

3.2 Macrostructural and microstructural analyses

Figure 3 shows the macrostructural view of the cross sections of the welding joints. The macro cross sections of the welding joints consisted of three parts: AZ31B alloy, A7075-T651 alloy, and ER5356 Al nugget. Although most nuggets were fully constructed, filling the spaces in the through holes of the A7075-T651 and AZ31B parent alloys, some nuggets were not. This condition might be due to the difference in the viscosity levels of the molten Al fillers at different welding powers. At a low welding power, the molten fillers exhibited increased viscosity and decreased fluidity because of the low welding heat. Consequently, they showed reluctance in spreading to fill the through holes. By contrast, at a high welding power, the molten fillers exhibited decreased viscosity and increased fluidity because of the high welding heat. Thus, the molten filler could more easily spread to fill the through holes at a high welding power than at a low welding power [31].

Mg alloys possess lower melting temperatures than Al, and they are highly reactive at elevated temperatures [31]. Therefore, some materials around the through holes on the AZ31B parent alloy side melted and occupied the spaces in the through holes during welding. Initiating the arc welding at the hole periphery rather than at the center of the holes is the cause of this occurrence. However, this condition is an uncontrollable incident in welding and is probably another reason why some nuggets were not fully constructed in the intervening layers. Some burn-throughs were also observed in the welding cross sections with incomplete nuggets; thus, the fillers could not fill the gaps in these sections. The welding macro cross sections of the joints with complete and incomplete nuggets are shown in Fig. 3a, b.

Al and Mg alloys also possess low solubility in each other [23, 32]. Therefore, the presence of any metallurgical bonding between the filler and AZ31B alloy in the welding joints cannot be definitively determined by macrostructural observation alone. However, a certain metallurgical bonding is believed to be present between the Al nuggets and AZ31B parent alloy. In the welding joints between any Al and Mg alloys with any Al filler, the formation of brittle Al_mMg_n IMCs is a common phenomenon. SEM and EDX analyses were performed to investigate the mechanisms of metallurgical bonding and the formation of Al_mMg_n IMCs in the welding joints, and details of which are described in Section 3.5. Figure 4 shows the microstructures at different locations of the welding cross sections shown in Fig. 3a, b.

The microstructures in the welding cross sections are shown in Fig. 4a–e. Figure 4a, c show the microstructure on the A7075-T651 alloy side. Figure 4b, d show the microstructure on the AZ31B alloy side. Figure 4e shows the overall microstructure of the Al nugget. Two types of microstructures of the A7075-T651 alloy were observed. The microstructure of the unaffected A7075-T651 parent alloy is shown in Fig. 4a, and that of the PMZ is shown in Fig. 4b. The HAZ was not distinguishable or might have existed along with PMZ. Thus, the HAZ was not shown in the figure. The grains in the microstructure of the PMZ of the A7075-T651 alloy recrystallized; thus, the grains increased in size. The grain boundary became shaggy compared with that of the parent alloy because of the effects of welding heat. The microstructure showed that the grains in the PMZ of the A70750-T651 alloy were equiaxed. The PMZ contained some microvoids and most probably minute amounts of Al_mFe_n and Al_nMn_m compounds.

By contrast, two microstructures were observed on the AZ31B alloy side: those of the unaffected AZ31B parent alloy, as shown in Fig. 4b, and the PMZ of the AZ31B alloy. The HAZ might have existed along with the PMZ and was

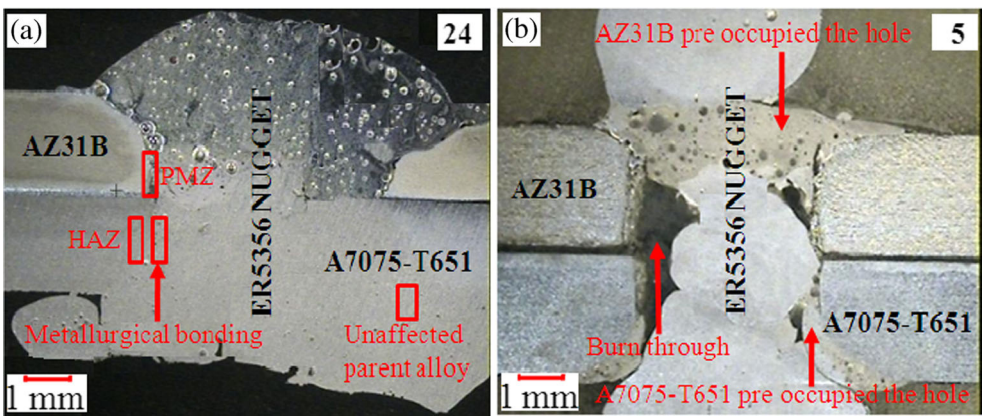

Fig. 3 Welding macro cross sections. **a** With complete nugget. **b** With incomplete nugget

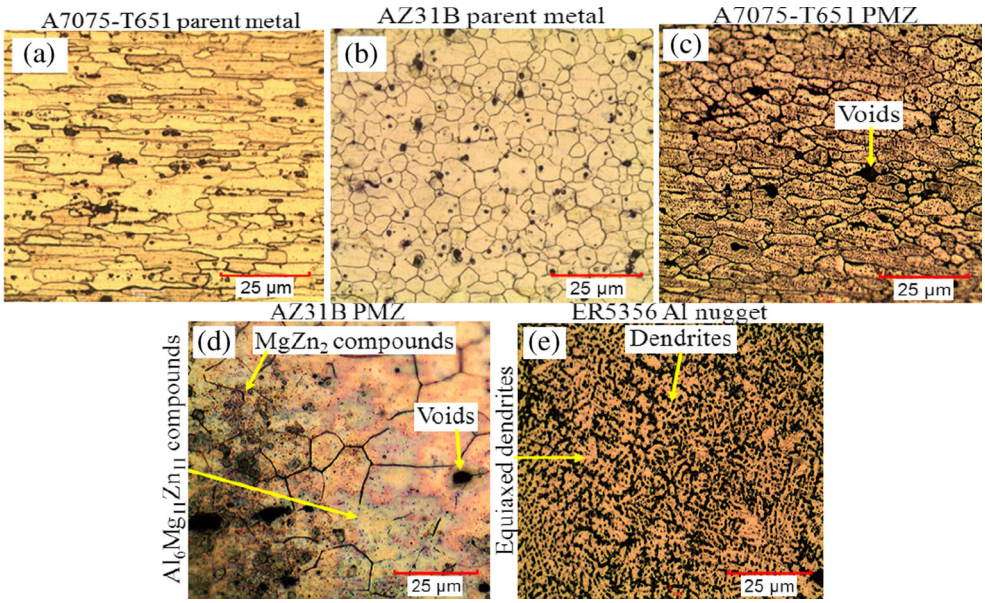

Fig. 4 Microstructure at welding cross section **a** at A7075-T651 parent alloy, **b** at AZ31B parent alloy, **c** at PMZ of A7075-T651 alloy, **d** at PMZ of AZ31B alloy, and **e** at Al nugget

unapparent. The microstructure of the PMZ was coarser than that of the parent alloy because of the effect of the welding heat. The grayish-black phases in the PMZ on the AZ31B alloy side were probably $MgZn_2$ and $Al_6Mg_{11}Zn_{11}$ compounds in accordance with the element compositions of the AZ31B parent alloy and ER5356 Al filler [33]. Some large microvoids were also observed. The microstructures of the ER5356 Al nugget showed almost the same features throughout the entire nugget area, with minimal differences in grain sizes. This condition might be due to different cooling rates at different parts of the Al nugget at the time of solidification. As shown in Fig. 4e, the dendrites were dominant in the Al nugget, and some equiaxed dendrites also existed.

3.3 Location of failure

Two types of fractures occurred during tensile and impact toughness testing. During tensile testing, 25 joints fractured in the Al nugget, and only 1 joint fractured in the AZ31B parent alloy. During impact toughness testing, 16 joints fractured in the Al nugget and 10 joints fractured in the AZ31B parent alloy. The fracture surface morphologies in the different fracture locations were investigated by SEM and analyzed by EDX to reveal the facts and features of the fracture in the AZ31B alloy and Al nugget, and details of which are discussed in Section 3.4. The fracture locations of all joints during tensile and toughness testing are listed in Table 3.

3.4 Fracture surface morphology

The SEM images of the fracture surface of the AZ31B alloy during tensile and toughness testing are shown in Fig. 5. The fracture surface of the unaffected AZ31B parent alloy was composed of cleavage planes, cleavage steps, and cloudy dimples. The cleavage planes were small, and the cleavage rivers were short and unapparent. Few inherent microvoids and cracks were also present. The fracture surface in the PMZ of the AZ31B alloy contained large microvoids, micropores, cracks, and oxides. The AZ31B alloy exhibited more sensitivity to the welding heat; as a result, pores, voids, cracks, and oxidation occurred in this alloy. As shown in Fig. 5, the fracture surface in the PMZ of the AZ31B alloy side contained some oxides that were introduced during welding because of the strong affinity of Mg to oxygen. The presence of pores has detrimental effects on the ductility of materials and is one of the causes of cracks and brittle fractures, which commonly occur during Mg welding [8]. Oxides promote the formation of more cracks and reduce bending elongation. Thus, during tensile and toughness testing, the pores, cracks, and oxides introduced during welding were broken up further and

Table 3 Location of fracture for tensile and charpy test

Fracture location																										
Exp. No.	1	2	3	4	5	6	7	8	9	10	11	12	13	14	15	16	17	18	19	20	21	22	23	24	25	26
Tensile Test	N	N	N	N	N	M	N	N	N	N	N	N	N	N	N	N	N	N	N	N	N	N	N	N	N	N
Toughness Test	M	N	M	N	N	M	N	N	M	N	N	N	M	N	M	M	N	N	N	N	N	M	N	M	M	N

N ER5356 Al nugget, *M* AZ31B Magnesium alloy

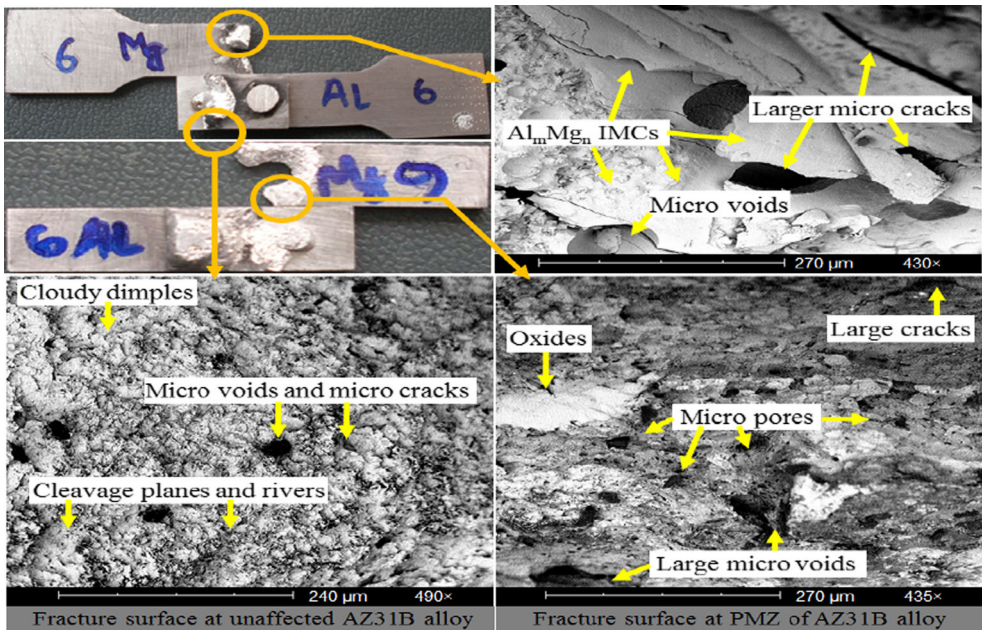

Fig. 5 SEM images of fracture surface at AZ31B alloy

distributed in a scattered mode. The formation of brittle Al_mMg_n IMCs is normal on the AZ31B alloy side if welded with an Al-based filler. These IMCs reduce the effective load-bearing area [34, 35]. During tensile and toughness testing, the inconsistent deformation of Al_mMg_n IMCs and oxides in the PMZ along with the inherent microvoids, micropores, and microcracks caused stress concentrations in the matrices and combined to form large cracks. As a result, the AZ31B alloy was affected more severely than the A7075-T651 alloy and ER5356 Al nugget by the pores, cracks, oxides, and brittle Al_mMg_n IMCs. This condition easily promoted crack propagation in the AZ31B alloy during tensile and toughness testing; as a result, fracture occurred in this alloy.

EDX analysis was performed at different fracture surface locations in the PMZ of the AZ31B alloy to determine the facts and features of the fracture in the zone, as shown in Fig. 6. Table 4 shows graphically and numerically the atomic percentages of the elements at points 1, 2, and 3 of the fracture surface in the PMZ of the AZ31B alloy. The analysis revealed that the fracture surface of AZ31B alloy mainly contained Mg (96.167 %), Al (2.050 %), Mn (1.462 %), Zn (0.283 %), Si (0.028 %), Ca (0.006 %), and Fe (0.005 %). These elements are the alloying elements normally present in the AZ31B alloy. The main elements in this zone were Mg, O, and Al. Al and Mg were mainly from the ER5356 Al filler and AZ31B parent alloy, respectively. The atomic percentages of Mg were 69.394 and 50.186 % at points 2 and 3, respectively. The atomic percentages of Al were 9.538 and 48.336 % at points 2 and 3, respectively. The atomic percentage of O was 19.673 % at point 2. Therefore, the element analysis results

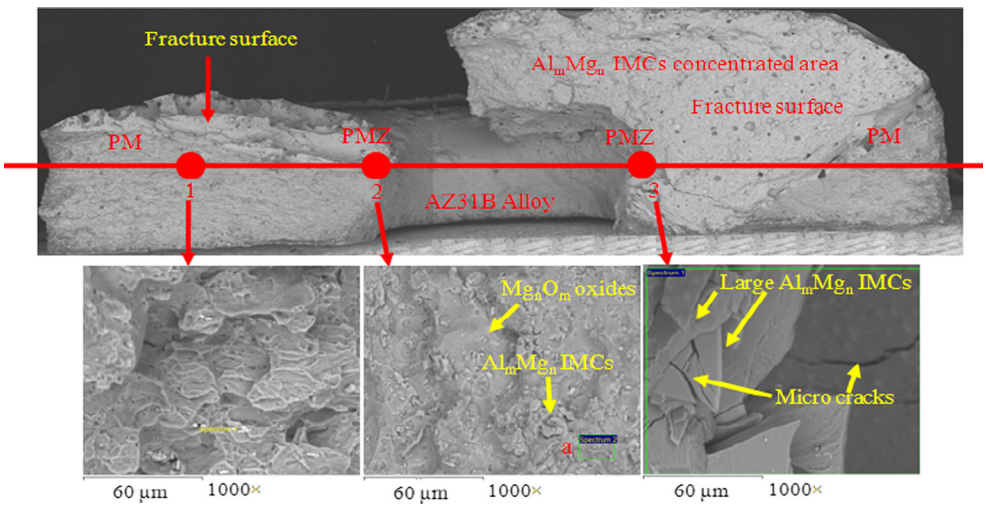

Fig. 6 EDX at different locations of AZ31B alloy fracture surface (with Al filler)

Table 4 EDX results of unaffected AZ31B alloy (point 1) and AZ31B alloy PMZ (point 2 and point 3) fracture surface

Elements	Atomic %		
	Point 1	Point 2	Point 3
Magnesium	96.167	69.394	50.186
Oxygen	–	19.673	–
Aluminum	2.050	9.538	48.336
Silicon	0.028	–	–
Calcium	0.006	–	0.151
Manganese	1.462	0.120	–
Iron	0.005	–	0.162
Zinc	0.283	–	0.656
Sodium	–	0.378	–
Gallium	–	0.304	–
Titanium	–	–	0.228
Chromium	–	–	0.170
Nickel	–	–	0.110

showed that good amounts of Al_mMg_n IMCs and magnesium oxide (Mg_nO_m) were present in the PMZ of the AZ31B alloy, thereby causing the fracture on the AZ31B alloy side.

Figure 7 shows the SEM images of the fracture surface of the ER5356 Al nugget. The failure occurring in the Al nuggets was caused by the incomplete formation of nuggets in the intervening layers during double-sided welding, as shown in Fig. 3b. The diffusion of some melted AZ31B alloy in the intervening layers of the nugget also caused the formation of a large amount of brittle Al_mMg_n IMCs [36]. Moreover, large microvoids, cracks, aluminum oxides (Al_mO_n), and Mg_nO_m were also present, causing crack initiation. As a result, the propagation of large cracks occurred during tensile and toughness testing. Furthermore, a highly brittle fracture mechanism was present in the core of the Al nuggets because of the formation of large voids, cracks, oxides, and a large amount of Al_mMg_n IMCs. These factors combined with the incomplete formation of some nuggets, resulting in the relative weakness of the Al nuggets compared with the A7075-T651 and AZ31B alloys and the fracture in the Al nugget.

Table 5 graphically and numerically shows the atomic percentages of the elements at two points of the fracture surface of the Al nugget. The EDX analysis locations at point 1 and 2 are shown in Fig. 8. The main elements in this zone were Al, Mg, and O. Al and Mg clearly originated from the ER5356 Al filler and AZ31B parent alloy, respectively. The atomic percentages of the elements were as follows: 53.327 % (Al), 24.859 % (O), and 21.332 % (Mg) at point 1; 62.921 % (Al), 31.856 % (Mg), and 4.774 % (O) at point 2.

Therefore, as shown in the element analysis, good amounts of brittle Al_mMg_n IMCs, Al_mO_n, and Mg_nO_m formed in the intervening layers of an Al nugget. Mg_nO_m resembled a blister. Some macrovoids also formed. The macrovoids, Al_mMg_n IMCs, and oxides stimulated the formation and propagation of large cracks in the ER5356 Al nuggets during tensile and toughness testing, thereby causing a fracture.

3.5 EDX analysis on metallurgical bonding

The welding cross section shown in Fig. 9 presents the metallurgical bonding between the parent alloys and ER5356 Al nugget. The bonding between the AZ31B alloy and Al nugget,

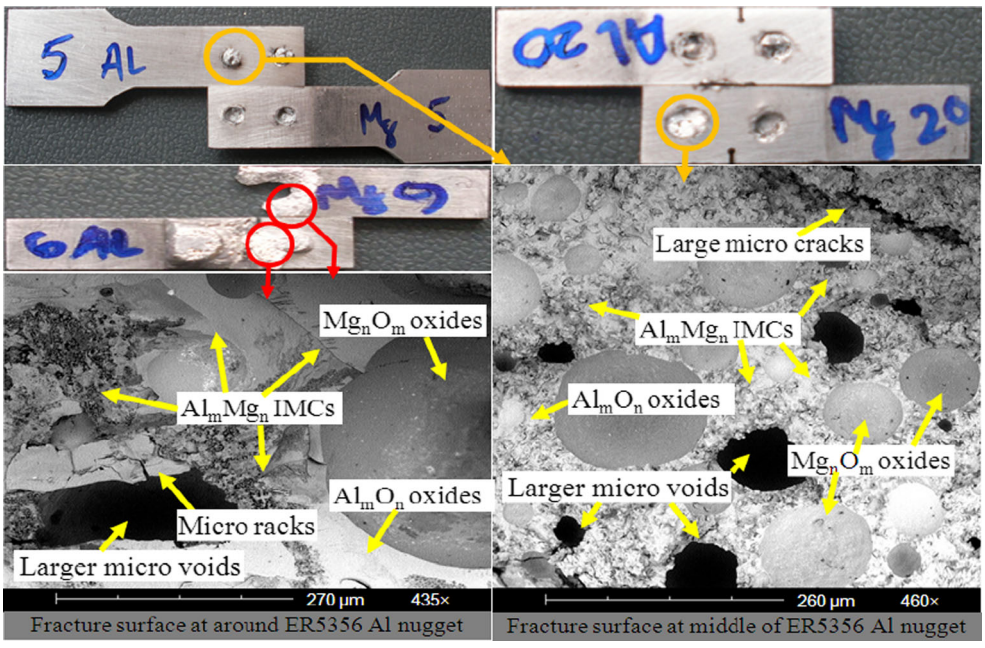

Fig. 7 SEM images of fracture surface at ER5356 Al nugget

Table 5 EDX results of ER5356 Al nugget fracture surface

Elements	Atomic %	
	Point 1	Point 2
Oxygen	24.859	4.774
Magnesium	21.332	31.856
Aluminum	53.327	62.921
Silicon	0.136	0.037
Zinc	0.346	0.412

which was approximately 20–40-μm thick, was rugged. By contrast, the bonding between A7075-T651 alloy and Al nugget was very smooth and thin, measuring approximately 2–3-μm thick. Table 6 presents the EDX-derived atomic percentages of the elements at points 1 and 2 of the AZ31B/Al nugget bonding. The EDX analysis results revealed that the AZ31B/Al bonding mostly contained Mg, Al, O, Si, and Zn. The Mg elements were from the AZ31B alloy, whereas the Al, Si, and Zn elements were definitely from the Al filler. The O elements were introduced during welding. Numerous macropores were present in the Al nugget on the AZ31B side. Based on the EDX analysis results on the atomic percentages of the elements, a large amount of Al_mMg_n IMCs and minute amounts of Al_mO_n and Mg_nO_m were present in the bonding.

Table 7 presents the EDX-derived atomic percentages of the elements at points 1 and 2 of the A7075-T651/Al nugget bonding. The A7075-T651/Al nugget bonding mostly contained Al, C, Mg, and O. Al was from both the A7075-T651 parent alloy and ER5356 Al filler. Mg was from the ER5356 Al filler, which had a high Mg content (~5 %). C and O elements were introduced during welding. According to the atomic ratio, minute amounts of aluminum carbide (Al_mC_n) compounds, Al_mO_n, and Mg_nO_m were present in the A7075-T651/Al nugget bonding. Few microcracks and micropores were also present. No fracture occurred in either the AZ31B/Al nugget or the A7075-T651/Al nugget bonding during tensile and toughness testing.

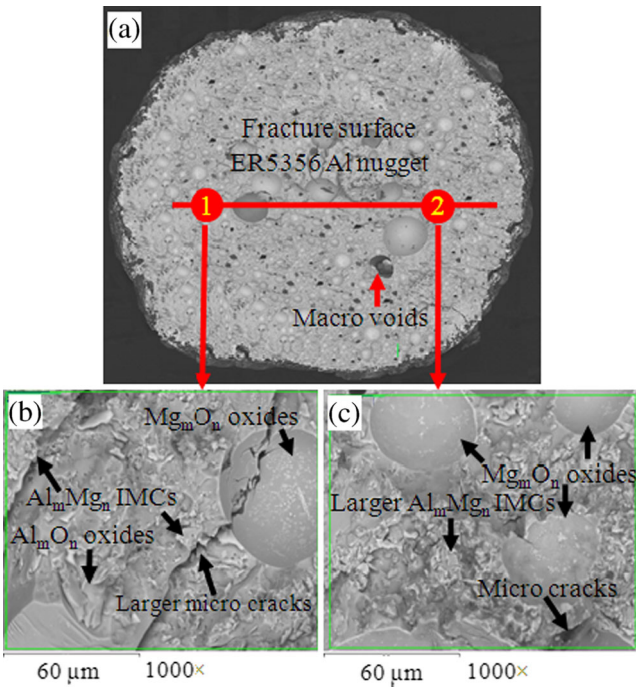

Fig. 8 EDX analysis at fracture surface at ER5356 Al nugget

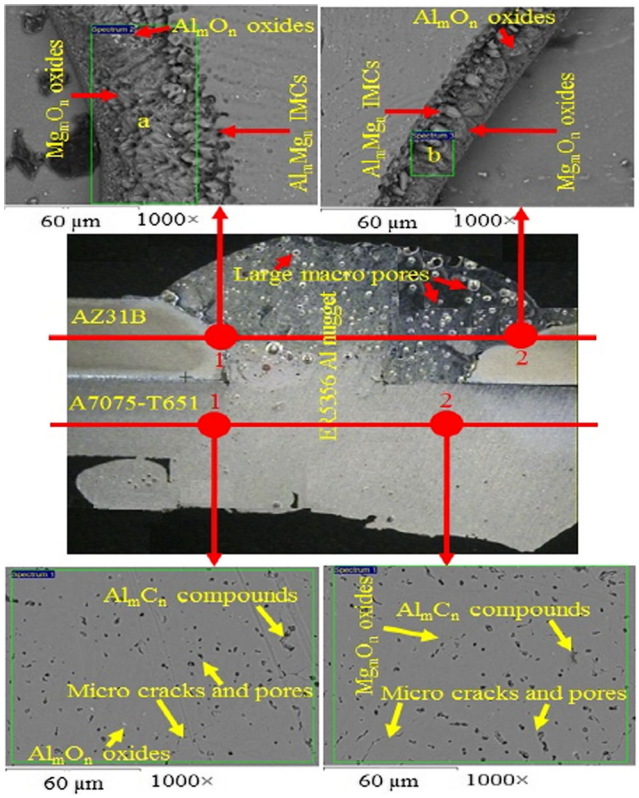

Fig. 9 EDX at AZ31B/ER5356 nugget and A7075-T651/ER5356 nugget bonding

Table 6 EDX results at point 1 and 2 at AZ31B/ER5356 Al nugget bonding and at ER5356 Al nugget/AZ31B alloy bonding respectively

Elements	Atomic %	
	Point 1	Point 2
Oxygen	–	28.119
Magnesium	55.336	50.117
Aluminum	40.981	18.732
Silicon	1.314	0.490
Zinc	1.146	0.320
Calcium	0.915	0.924
Manganese	0.199	0.333
Iron	–	0.295
Nickel	–	0.617

Table 7 EDX analysis at point 1 and point 2 of A7075-T651/Al nugget bonding

Elements	Atomic %	
	Point 1	Point 2
Carbon	18.011	17.085
Oxygen	3.166	2.268
Magnesium	4.334	4.469
Aluminum	73.427	75.844
Zinc	0.103	0.149

4 Conclusion

i. A7075-T651 and AZ31B dissimilar alloys were successfully lap-welded by a new technique called GMA plug welding method using an ER5356 Al filler. Significantly improved mechanical properties were achieved. The welding parameters 15 L/min GSR, 8 mm TWD, 15 V WV, and 115 A WC were considered optimal because they allowed for the highest tensile strength and a good impact toughness. The maximum YS, UTS, and impact toughness of the joints were 97.830 MPa, 226.28 MPa (89 % of the UTS of the AZ31B parent alloy), and 7.42 J (84 % of the impact toughness of the AZ31B parent alloy), respectively. Therefore, the objective of achieving significantly enhanced mechanical properties of the joint by reducing the direct bonding area between A7075-T651 and AZ31B alloys by using the ER5356 Al filler was satisfied by the proposed GMA plug welding method.

ii. Although most nuggets were fully constructed, filling the spaces in the through holes in the A7075-T651 and AZ31B parent alloys, some nuggets were not. This condition occurred because of the differences in the viscosity and fluidity levels of the molten fillers at different welding powers. Certain AZ31B materials melted and occupied the spaces in the through holes during welding given that Mg alloys have lower melting temperatures than Al. Initiating the arc welding at the hole periphery rather than at the center of the holes was the reason for this occurrence. Some burn-throughs were also observed in the welding cross sections with incomplete nuggets. The grains in the microstructure of the PMZs of the A7075-T651 and AZ31B alloys were recrystallized; as a result, the grains increased in size, and the grain boundary became shaggy compared with that of the parent alloy because of the effects of the welding heat. The grains in the microstructure of the PMZ of the A70750-T651 alloy were equiaxed, and this PMZ might have contained minute amounts of Al_mFe_n and Al_nMn_m compounds along with some microvoids. The grayish-black phases in the PMZ on the AZ31B alloy side were probably $MgZn_2$ and $Al_6Mg_{11}Zn_{11}$ compounds. Some large microvoids were observed. The microstructures of the ER5356 Al nugget showed almost the same features throughout the entire nugget area.

iii. A total of 25 joints failed in the Al nugget, and only 1 joint failed in the AZ31B parent alloy during tensile testing. A total of 16 joints failed in the Al nugget and 10 joints failed in the AZ31B parent alloy during impact toughness testing. Most of the failures occurred in the Al nugget because cracks initiated as a result of the large amounts of Al_mO_n, Mg_nO_m, and brittle Al_mMg_n IMCs; micropores; voids; and cracks. No joints failed in the A7075-T651 parent alloy. The EDX analysis results revealed that a fair amount of Al_mMg_n IMCs were observed in the cross sections of the joints especially between the Al nugget and the AZ31B parent alloy. However, the amount was definitely significantly lower than that generated by other welding techniques because the bonding area between A7075-T651 and AZ31B dissimilar alloys was less in the proposed technique. Therefore, the joints formed by the proposed technique showed better mechanical performance (strength and toughness) than those by other welding techniques.

iv. The thickness of the AZ31B/Al nugget bonding and that of the A7075-T651/Al nugget bonding were approximately 2–3 μm and 20–40 μm, respectively. These layers mostly contained brittle Al_mMg_n IMCs, Al_mO_n, Mg_nO_m, Al_mC_n compounds, and some micropores and voids. No evidence of fracture occurring in these bonding areas could be revealed by tensile and toughness testing.

Acknowledgments The authors would like to thank the Ministry of Education of Malaysia for funding this study through the FRGS research (RDU140118) and the Faculty of Mechanical Engineering, University Malaysia Pahang for providing the laboratory facilities needed to accomplish this study.

References

1. Karunakaran N, Balasubramanian V (2011) Effect of pulsed current on temperature distribution, weld bead profiles and characteristics of gas tungsten arc welded aluminum alloy joints. Trans Nonferrous Metals Soc China 21(2):278–286. doi:10.1016/s1003-6326(11)60710-3
2. Hayat F (2011) The effects of the welding current on heat input, nugget geometry, and the mechanical and fractural properties of resistance spot welding on Mg/Al dissimilar materials. Mater Des 32(4):2476–2484
3. Zhang HT, Song JQ (2011) Microstructural evolution of aluminum/magnesium lap joints welded using MIG process with zinc foil as an interlayer. Mater Lett 65(21–22):3292–3294. doi:10.1016/j.matlet.2011.05.080
4. X-d Q, L-m L (2012) Fusion welding of Fe-added lap joints between AZ31B magnesium alloy and 6061 aluminum alloy by hybrid laser–tungsten inert gas welding technique. Mater Des 33:436–443
5. Yan YB, Zhang ZW, Shen W, Wang JH, Zhang LK, Chin BA (2010) Microstructure and properties of magnesium AZ31B–

aluminum 7075 explosively welded composite plate. Mater Sci Eng A 527(9):2241–2245. doi:10.1016/j.msea.2009.12.007
6. Pieta G, dos Santos J, Strohaecker T, Clarke T (2013) Optimization of friction spot welding process parameters for AA2198-T8 sheets. Mater Manuf Process 29(8):934–940, just-accepted
7. Hu H, Yu A, Li N, Allison JE (2003) Potential magnesium alloys for high temperature die cast automotive applications: a review. Mater Manuf Process 18(5):687–717
8. Mofid M, Abdollah-Zadeh A, Malek Ghaini F (2012) The effect of water cooling during dissimilar friction stir welding of Al alloy to Mg alloy. Mater Des 36:161–167
9. Chen Y, Nakata K (2008) Friction stir lap joining aluminum and magnesium alloys. Scr Mater 58(6):433–436
10. Kwon Y, Shigematsu I, Saito N (2008) Dissimilar friction stir welding between magnesium and aluminum alloys. Mater Lett 62(23):3827–3829
11. Liu C, Chen D, Bhole S, Cao X, Jahazi M (2009) Polishing-assisted galvanic corrosion in the dissimilar friction stir welded joint of AZ31 magnesium alloy to 2024 aluminum alloy. Mater Charact 60(5):370–376
12. Chen YC, Nakata K (2008) Friction stir lap joining aluminum and magnesium alloys. Scr Mater 58(6):433–436. doi:10.1016/j.scriptamat.2007.10.033
13. Mofid MA, Abdollah-zadeh A, Malek Ghaini F (2012) The effect of water cooling during dissimilar friction stir welding of Al alloy to Mg alloy. Mater Des 36:161–167. doi:10.1016/j.matdes.2011.11.004
14. Casalino G (2007) Statistical analysis of MIG-laser CO2 hybrid welding of Al–Mg alloy. J Mater Process Technol 191(1–3):106–110. doi:10.1016/j.jmatprotec.2007.03.065
15. Chang W-S, Rajesh S, Chun C-K, Kim H-J (2011) Microstructure and mechanical properties of hybrid laser-friction stir welding between AA6061-T6 Al alloy and AZ31 Mg alloy. J Mater Sci Technol 27(3):199–204
16. Yan J, Xu Z, Li Z, Li L, Yang S (2005) Microstructure characteristics and performance of dissimilar welds between magnesium alloy and aluminum formed by friction stirring. Scr Mater 53(5):585–589
17. Shang J, Wang K, Zhou Q, Zhang D, Huang J, Li G (2012) Microstructure characteristics and mechanical properties of cold metal transfer welding Mg/Al dissimilar metals. Mater Des 34:559–565
18. Yan Y, Zhang Z, Shen W, Wang J, Zhang L, Chin B (2010) Microstructure and properties of magnesium AZ31B–aluminum 7075 explosively welded composite plate. Mater Sci Eng A 527(9):2241–2245
19. Liu X-H, Gu S-H, Wu R-Z, Leng X-S, Yan J-C, Zhang M-L (2011) Microstructure and mechanical properties of Mg-Li alloy after TIG welding. Trans Nonferrous Metals Soc China 21(3):477–481
20. Tabasi M, Farahani M, Givi MKB, Farzami M, Moharami A (2015) Dissimilar friction stir welding of 7075 aluminum alloy to AZ31 magnesium alloy using SiC nanoparticles. Int J Adv Manuf Technol. doi:10.1007/s00170-015-8211-y, 1–11
21. Pokataev E, Trykov YP (2004) Residual stresses in magnesium–aluminium composites, produced by explosive welding. Weld Int 18(8):656–659
22. Carlone P, Astarita A, Palazzo GS, Paradiso V, Squillace A (2015) Microstructural aspects in Al–Cu dissimilar joining by FSW. Int J Adv Manuf Technol 79(5):1109–1116. doi:10.1007/s00170-015-6874-z
23. Zhang H, Song J (2011) Microstructural evolution of aluminum/magnesium lap joints welded using MIG process with zinc foil as an interlayer. Mater Lett 65(21):3292–3294
24. Ishak M, Maekawa K, Yamasaki K (2012) The characteristics of laser welded magnesium alloy using silver nanoparticles as insert material. Mater Sci Eng A 536:143–151
25. Cao R, Wen B, Chen J, Wang P-C (2013) Cold metal transfer joining of magnesium AZ31B-to-aluminum A6061-T6. Mater Sci Eng A 560:256–266
26. Temmar M, Hadji M, Sahraoui T (2011) Effect of post-weld aging treatment on mechanical properties of tungsten inert gas welded low thickness 7075 aluminium alloy joints. Mater Des 32(6):3532–3536. doi:10.1016/j.matdes.2011.02.011
27. Tarpani JR, Maluf O, Gatti MCA (2009) Charpy impact toughness of conventional and advanced composite laminates for aircraft construction. Mater Res 12(4):395–403
28. Erturk MT (2011) Microstructural and mechanical characterization of metal active gas welded joint between cast iron and low carbon steel. Master's Thesis, Middle East Technical University
29. Padmanaban G, Balasubramanian V (2011) Effects of laser beam welding parameters on mechanical properties and microstructure of AZ31B magnesium alloy. Trans Nonferrous Metals Soc China 21(9):1917–1924
30. Simoncini M, Forcellese A (2012) Effect of the welding parameters and tool configuration on micro- and macro-mechanical properties of similar and dissimilar FSWed joints in AA5754 and AZ31 thin sheets. Mater Des 41:50–60
31. Hirano S, Okamoto K, Doi M, Kamura O, Inagaki M, Aono Y (2004) Microstructure of the interface in magnesium alloy to aluminium alloy dissimilar joints produced by friction stir welding. Weld Int 18(9):702–708
32. Miao Y, Han D, Yao J, Li F (2010) Effect of laser offsets on joint performance of laser penetration brazing for magnesium alloy and steel. Mater Des 31(6):3121–3126
33. Liu F, Ren D, Liu L (2013) Effect of Al foils interlayer on microstructures and mechanical properties of Mg–Al butt joints welded by gas tungsten arc welding filling with Zn filler metal. Mater Des 46:419–425
34. Li J-F, Z-w P, Li C-X, Jia Z-Q, W-j C, Zheng Z-Q (2008) Mechanical properties, corrosion behaviors and microstructures of 7075 aluminium alloy with various aging treatments. Trans Nonferrous Metals Soc China 18(4):755–762
35. Liu F, Wang H, Liu L (2014) Characterization of Mg/Al butt joints welded by gas tungsten arc filling with Zn–29.5 Al–0.5 Ti filler metal. Mater Charact 90:1–6
36. Liu L, Ren D (2011) A novel weld-bonding hybrid process for joining Mg alloy and Al alloy. Mater Des 32(7):3730–3735